Solvent Effects on the UV ($n \rightarrow \pi^*$) and NMR (^{13}C and ^{17}O) Spectra of Acetone in Aqueous Solution. An Integrated Car−Parrinello and DFT/PCM Approach

Orlando Crescenzi,[†] Michele Pavone,[†] Filippo De Angelis,[‡] and Vincenzo Barone*[,†]

Dipartimento di Chimica, Università di Napoli "Federico II", Complesso Universitario di Monte Sant'Angelo, Via Cintia, I-80126 Napoli, Italy, and Istituto CNR di Scienze e Tecnologie Molecolari (ISTM), Dipartimento di Chimica, Università di Perugia, via Elce di Sotto 8, I-60123 Perugia, Italy

Received: August 14, 2004

The accurate reproduction of ultraviolet and nuclear magnetic resonance spectra of acetone in aqueous solution is used as a test of an integrated computational tool rooted in the density functional theory, the polarizable continuum model, and the Car−Parrinello dynamics. The analysis and solution of several conceptual and practical issues results in a robust and effective approach, which also can be used by nonspecialists and provides a general and powerful complement to experimental techniques.

1. Introduction

The ab initio computation of spectroscopic parameters has been used for a long time to aid/support the interpretation of experimental data for small molecules:[1] one could just cite the fields of matrix isolation of reactive species and gas-phase photochemistry as examples of traditionally fruitful cooperation between experimentalists and theoretical chemists. With the development of linear scaling procedures[2] rooted in the framework of density functional theory (DFT),[3] rapid and accurate computations of spectroscopic parameters for medium-sized molecules in vacuo are rapidly becoming routine. Thus, for example, the introduction of time-dependent DFT (TD-DFT)[4] allows, in many cases, reliable computation of electronic excitation energies, whereas the gauge-including atomic orbitals (GIAO) formalism,[5] combined with a DFT approach, has proven particularly effective in reproducing nuclear magnetic resonance (NMR) chemical shifts.[6] As a consequence of the steady increase in the size of molecules that are amenable to ab initio prediction of spectroscopic parameters, a correspondingly larger part of the chemical community is coming into contact with applications that were, in the past, the domain of specialists.[6,7]

However, the vast majority of experimental NMR and ultraviolet (UV) spectra are actually recorded in solution. As a matter of fact, condensed phases represent the natural physical environment for many chemical systems, ranging from living cells to composite materials and industrial catalysts. To predict the physical and chemical behavior of molecules in condensed phases accurately, many subtle effects induced by the complex chemical environment (e.g., the solvent) must be taken into consideration.[8]

In principle, it is possible to include large parts of the environment (e.g., a large number of solvent molecules) within the system that is treated at the quantum mechanical (QM) level.[9]

Even if the size of systems amenable to full QM description is increasing steadily, such a brute force approach is quite unattractive, especially considering that spectroscopic parameters such as UV excitation energies and NMR chemical shifts are second-order response properties, whose calculation requires considerable computational effort.[10]

These difficulties are magnified when one wishes to take into account the dynamics of the system. This is often necessary, because some spectroscopic parameters are quite sensitive to the precise geometrical features not only of the core molecular system, but also of the embedding chemical environment.

In many cases, a very attractive solution is represented by implicit solvation models, the best known of which is the polarizable continuum model (PCM).[11] In this approach, the solute molecule is embedded in a cavity formed by the envelope of spheres centered on solute atoms or atomic groups; inside the cavity, the relative dielectric constant is equal to 1, as in a vacuum, whereas it takes the solvent bulk value (e.g., 78.39 for water) outside the cavity. The solvent medium, after it has been polarized by the presence of the solute, perturbs the embedded molecule by a reaction field, which is described in terms of a pattern of effective charges on the cavity surface. Starting from this definition, very efficient linear scaling procedures have been implemented for cavity construction and evaluation of energy and of its first and second derivatives, with respect to geometrical, electric, and magnetic parameters.[12]

However, implicit solvation models may fail to correctly reproduce the effects of highly specific solute−solvent interactions, such as hydrogen bonds, on spectroscopic parameters.[1d,13] Traditionally, the issue has been addressed by including, within the system that is described at the QM level, a few solvent molecules positioned at specific locations around the solute.[1d,14] To apply such a cluster/continuum approach, one, first of all, must define the cluster size required to reach convergence in the computed spectroscopic parameters; moreover, if dynamical effects are important, different cluster sizes/geometries will also need to be explored, and the resulting calculations will need to be properly averaged. Although the central solute molecule will certainly be treated at a high QM level, the explicit solvent molecules might be treated at a lower theory level, maybe even in terms of classical point charges. To take into account the further portions of the solvent, the PCM can still be brought into play; as an alternative, a large number of molecular mechanical (MM) charges may be used.[15]

* Author to whom correspondence should be addressed. E-mail: baronev@unina.it.

[†] Università Federico II.

[‡] ISTM−Perugia.

10.1021/jp046334i CCC: $30.25
Published on Web 12/13/2004

The choice among all the alternative/complementary approaches previously suggested is not a simple one. First of all, the performances will obviously be dependent on the actual chemical system at hand; moreover, given the widely different sensitivity of the various types of spectroscopic parameters to specific environmental effects, a protocol that provides satisfactory results in the computation of a certain spectroscopic property may well turn out to be far from ideal in the prediction of another type of spectral parameter. This prompted us to start a comprehensive research program that is directed toward the development and validation of a general and effective computational protocol for the QM computation of spectroscopic parameters for large molecules in condensed phases. As a first step, we have performed a theoretical investigation of the solvent effect on the $n \rightarrow \pi^*$ electronic transition energy and on the ^{13}C and ^{17}O nuclear magnetic shieldings of the carbonyl group of the acetone molecule in aqueous solution. Acetone was chosen as a suitable benchmark, given its relatively high polarity and the availability of suitable experimental data. Of course, the system, by itself, is a chemically interesting one; moreover, it can also be regarded as a simple model to probe the general features of the carbonyl−water interaction, which is an issue of still wider chemical and biochemical interest.

The suggested computational approach is based on Car−Parrinello molecular dynamics (CPMD)[16] simulations of acetone in aqueous solution (and, for comparison, in the gas phase), which are then used as starting points for the evaluation of solvent/dynamical effects on spectroscopic parameters.

Previous simulations of this type on the acetone−water system have been conducted both at the full QM level[17] and with a QM/MM approach.[18] However, the computation of spectral properties was performed within the CPMD code; with this approach, the choice of DFT models is currently limited to functionals based on the generalized gradient approximation (GGA), which may not be optimal for reproduction of spectral properties.[19] In the present study, the computation of spectroscopic parameters was performed in a separate stage on a large number of frames extracted at regular intervals from the CPMD simulation: this allows us to use hybrid functionals (or any other suitable theory level) during the critical phase of the procedure, namely, the calculation of the spectroscopic property.

The CPMD approach has also proven successful for the computation of ^{17}O NMR shieldings in aqueous solution within the Car−Parrinello (CP) scheme[20a] and combined with Hartree−Fock density functional theory (HF-DFT) calculations of shielding tensor.[20b]

The paper is organized in the following way. The geometrical and energetic features of the structures derived from the two CPMD simulations, in the gas phase and in water, are analyzed first and compared to the results of optimizations performed at several different levels. Some general considerations on the influence of solvent on different spectroscopic parameters then are introduced, and the computational procedures required to reproduce such solvent effects are discussed. The following sections are devoted to the specific case of acetone $n \rightarrow \pi^*$ excitation energies and of ^{17}O and ^{13}C NMR shieldings. The concluding section summarizes the results and puts them in the more-general perspective of the computation of spectroscopic parameters in condensed phases.

2. Methods

2.1. Car−Parrinello Molecular Dynamics. First-principles simulations were conducted with the parallel version[21a] of the original CP code implementing Vanderbilt pseudo-potentials;[21b] the Perdew−Burke−Ernzerhof (PBE) exchange-correlation GGA functional was used.[22] Core states were projected, using "ultrasoft" pseudo-potentials generated according to the scheme proposed by Vanderbilt.[23] The wave function (density) was expanded in plane waves up to an energy cutoff of 25 (200) Ry; the equations of motion were integrated with a time step of 10 a.u. (0.242 fs), with an electronic fictitious mass of 1000 a.u. For the system in aqueous solution, the initial configuration was obtained by replacing a water molecule with an acetone molecule from a previously equilibrated liquid water trajectory obtained for a constant-volume cubic supercell including 64 water molecules at a density of 1.00 g/cm^3.[24a] The simulation in vacuo was performed, instead, starting from the optimized structure of acetone in a cubic cell with side of 12.41 Å. The considered systems have been equilibrated for 1.5 ps at 300 K, applying a Nosè thermostat,[25] which enforces a canonical (NVT) ensemble. After equilibration, the trajectories of the systems have been followed for 4.0 ps, during which statistical averages have been taken. The average temperature during the simulations in vacuo and in aqueous solution was 312 and 320 K, respectively. The present methodology has been recently shown to provide radial distribution functions (rdfs) of liquid water in good agreement with experimental data and with previous ab initio molecular dynamics simulations by Silvestrelli and Parrinello.[24]

TABLE 1: Geometrical Parameters of the Acetone Molecule, Averaged over the Car-Parrinello Molecular Dynamics (CPMD) Runs, and Experimental Values from Gas-Phase Electron Diffraction[a]

	CPMD runs		experimental
	gas phase	aqueous solution	gas phase
	Bond Distance (Å)		
C═O	1.23 (0.02)	1.25 (0.01)	1.210 (0.003)
C−C	1.52 (0.04)	1.50 (0.03)	1.507 (0.002)
C−H	1.11 (0.04)	1.11 (0.02)	1.076 (0.006)
	Bond Angle (deg)		
C−C═O	121.4 (4.3)	121.0 (3.4)	121.7[b]
C−C−C	116.9 (5.3)	117.4 (3.1)	116.7 (0.3)
C−C−H	110.1 (6.8)	110.3 (5.5)	111.7 (1.5)
H−C−H	108.4 (6.2)	108.4 (5.4)	
C−C═O···C	180.0 (6.8)	180.0 (8.7)	180.0[b]

[a] Values in parentheses represent the standard deviations. [b] Assumed value.

2.2. Cluster Calculations. Geometry optimizations, electronic transition energies, and NMR shieldings were computed with the C.02 release of the Gaussian03 package.[26] The minimum energy structure of the acetone molecule was computed using the PBE exchange and correlation functional, both in its pure GGA formulation[22] and within the hybrid HF-DFT scheme known as PBE0, where the PBE exchange term is corrected by an amount of 0.25 pure Hartree−Fock exchange.[27] The basis sets adopted belong to the Pople series,[28] either valence-double-ζ or valence-triple-ζ, possibly augmented with diffuse and polarization functions; in some calculations, the correlation consistent basis sets of Dunning were also used.[29] NMR shieldings were obtained by the GIAO procedure,[5] and electronic transition energies were computed by TD-DFT calculations.[4] The latest implementation[12] of the PCM[11] was used to account for bulk solvent effects, in combination with the UAHF set of atomic radii[12c] and a nonequilibrium formulation for UV spectroscopic parameters.[12d]

3. Results

3.1. Structural Analysis. Table 1 lists the geometrical parameters for acetone, averaged over the gas-phase and aqueous

TABLE 2: Geometrical Parameters for the Minimum Energy Structures of Acetone Computed in the Gas Phase at Different Theory Levels

	PBE/plane wave	PBE/6-31+G(d,p)	PBE0/6-31+G(d,p)	experimental gas phase[a]
		Bond Distance (Å)		
C=O	1.229	1.229	1.214	1.210 (0.003)
C−C	1.514	1.520	1.510	1.507 (0.002)
C−H	1.106	1.102	1.094	1.076 (0.006)
		Bond Angle (deg)		
C−C=O	121.6	121.7	121.7	121.7[b]
C−C−C	116.8	116.6	116.6	116.7 (0.3)

[a] Values in parentheses represent the standard deviations. [b] Assumed value.

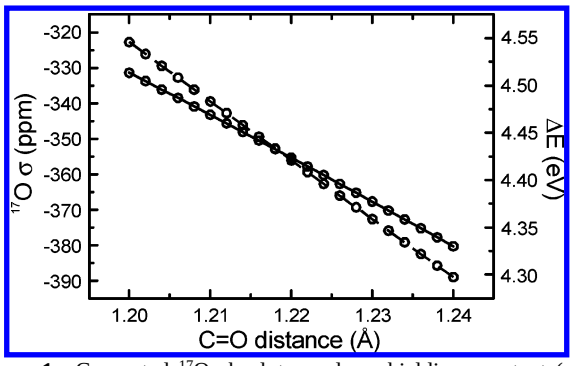

Figure 1. Computed ^{17}O absolute nuclear shielding constant (solid line) and $n \rightarrow \pi^*$ transition energy of the acetone molecule (broken line), each as a function of carbonyl bond length. The PBE0/6-311+G-(d,p) level of theory was used for each parameter.

solution CPMD, in comparison with the gas-phase experimental values obtained by electron diffraction spectroscopy.[30]

As far as gas-phase values are concerned, there is good agreement between the computed and experimental angles; however, the CPMD data seem to overestimate the bond distances by an amount of ∼0.02 Å. The ability of CPMD simulations to reproduce correct geometries, first of all, is associated with the theory level adopted in the electronic structure calculation. At the DFT level, the CP scheme with plane waves basis sets can be used efficiently only with GGA functionals[31] (in the present study, we actually used the PBE functional); thus, the overestimation of the average bond lengths can be traced back to the well-known limitations of GGA functionals.[19] The average carbonyl bond length computed from the CPMD is 1.23 ± 0.02 Å, in very good agreement with the results of a previous gas-phase CPMD simulation that was conducted at the BLYP level.[17,18]

Of course, the systematic error in bond lengths will have an impact on the computed spectroscopic parameters; thus, for example, Figure 1 shows the dependence of the computed ^{17}O absolute nuclear shielding constant (σ) and the $n \rightarrow \pi^*$ transition energy (ΔE) on the carbonyl bond length: an increase in length of 0.02 Å results in a ∼3% decrease of ΔE, and an even stronger decrease of σ, by ∼7%.

To quantify the intrinsic errors that are associated with use of the PBE functional, Table 2 compares the minimum-energy geometry computed at the PBE/plane waves level with those obtained using a medium-to-large-sized Gaussian basis set and either the PBE functional or its nonempirical hybrid counterpart, which is known as PBE0.

The geometry from the PBE Gaussian optimization using the 6-31+G(d,p) basis set corresponds strictly to that computed in plane waves; shifting from PBE to PBE0 in the Gaussian optimization, which amounts to an introduction of 25% Hartree−Fock exchange into the PBE functional, decreases the carbonyl bond distance to 1.214 Å, which is an improvement of 0.015 Å toward the experimental value of 1.210 Å.

TABLE 3: Geometrical Parameters of the Carbonyl−Water Hydrogen Bonds, Averaged over the CPMD Simulation

parameter	value[a]
number of hydrogen bonds	2.1
($O_{acetone}\cdots O_{water}$) distance	2.94 Å (0.20 Å)
($O_{acetone}\cdots H_{water}$) distance	1.99 Å (0.22 Å)
($H_{water}-O_{water}\cdots O_{acetone}$) angle	15.5° (8.0°)

[a] Values given in parentheses are standard deviations.

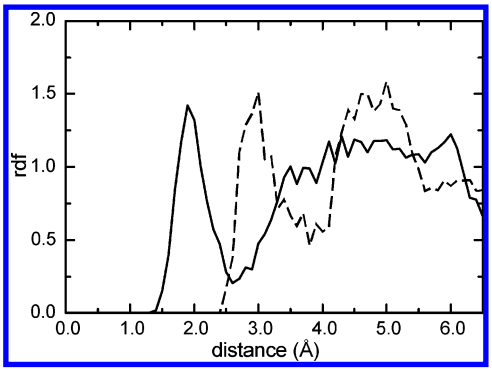

Figure 2. Radial distribution functions (rdfs) between the carbonyl oxygen and water oxygen (broken line) and hydrogen (continuous line).

If we turn now to the CPMD run in aqueous solution (Table 1), the average carbonyl bond length is 1.25 Å, and that for the C−C bond is 1.50 Å. Both lengths have increased by 0.02 Å, with respect to the corresponding gas-phase CPMD average values, as an effect of the solvent environment; by contrast, the bond angle values are essentially unaffected.

The arrangement of water molecules around acetone—and, in particular, hydrogen bonding to the carbonyl oxygen—is the other crucial structural parameter that must be quantified in the CPMD simulation. We adopted some simple and widespread geometrical criteria to identify hydrogen bonds,[32] namely

$$\text{distance}(O_{acetone}\cdots O_{water}) \leq 3.50 \text{ Å}$$

$$\text{distance}(O_{acetone}\cdots H_{water}) \leq 2.60 \text{ Å}$$

$$\text{angle}(H_{water}-O_{water}\cdots O_{acetone}) \leq 30°$$

With this definition, the average number of water molecules that were hydrogen-bonded to carbonyl oxygen was 2.1; Table 3 lists some average features of these hydrogen bonds.

Figure 2 depicts the rdfs between the carbonyl oxygen and water oxygen and hydrogen: the first peaks match the average values of Table 3 well.

Because the number of hydrogen bonds to acetone oxygen in individual CPMD frames ranges from zero to three, a more-detailed analysis of the water arrangement around the carbonyl was sought by extracting, from the frames, the first-, second-, and third-closest water molecules (in terms of the inter-oxygen distance), and repeating the same geometrical analyses on these

clusters. Over the total number of hydrogen bonds to the carbonyl oxygen, 45% involve the first-closest water molecule, 37% the second-closest water, and 18% the third-closest water. Conversely, although the first-closest water molecule is hydrogen-bonded 96% of the time, this probability drops to 80% for the second-closest water, and to 39% for the third-closest water. Thus, it appears that, in many cases, the second-closest water is actually not hydrogen-bonded to the carbonyl, whereas the third-closest water is; however, there are also cases of three genuine hydrogen bonds.

To go beyond this simple, but somewhat definition-dependent, geometrical analysis, we performed a more-general energetic analysis of the hydrogen-bond interactions. Reference total interaction energies have been taken from PBE/plane-wave optimized clusters (with all hydrogen bonds involving the carbonyl) and are 5.4 kcal/mol for acetone$-H_2O$, 11.4 kcal/mol for acetone$-(H_2O)_2$, and 14.8 kcal/mol for acetone$-(H_2O)_3$. Thirty eight frames, evenly spaced along the CPMD trajectory, were selected, and from each of them, the bare acetone molecule was extracted, as well as six different clusters, containing the first one, two, and three water molecules closest to the carbonyl oxygen, either with or without the central acetone molecule itself:

$$\text{acetone} + n\text{H}_2\text{O} \qquad (\text{for } n = 0, 1, 2, 3)$$

$$m\text{H}_2\text{O} \qquad (\text{for } m = 1, 2, 3)$$

All of these clusters were examined by single-point calculations at the PBE0/6-311+G(d,p) level, to decompose the overall interaction energy into partial contributions. The first water molecule is hydrogen-bonded to acetone in all but two cases (data not shown). The values of E(acetone + 1st H_2O + 2nd H_2O) − E(acetone) − E(1st H_2O + 2nd H_2O) reported in Figure 3A show that, by the energetic criterion, the two closest waters are both hydrogen-bonded to acetone, in most cases. A similar plot for the first three waters (Figure 3B) shows that, in most frames, the overall interaction energy lies just below the energetic level expected for two hydrogen bonds; however, there are some cases where the presence of a third acetone−water hydrogen bond is distinctly supported; few clusters with just one hydrogen bond or no hydrogen bond at all are also evident. Interestingly, from consideration of the interaction energies within the three-water clusters—E(1st H_2O + 2nd H_2O + 3rd H_2O) − E(1st H_2O) − E(2nd H_2O) − E(3rd H_2O), shown in Figure 3C—it appears that, apart from one single frame, there is no hydrogen bonding among these water molecules. In summary, both from geometrical analysis and from energetic analysis, we conclude that, on average two water molecules are hydrogen-bonded to the acetone carbonyl oxygen; moreover, in essentially all cases, three molecules of water should be sufficient to account for the entire hydrogen-bond network around the carbonyl.

Further insight into the solvent effects can be based on a decomposition into different factors. The first contribution is an indirect effect, because of the geometrical rearrangement that the solute molecule undergoes when immersed in the solvent environment; a second, direct effect is, instead, associated with the perturbation of the solute Hamiltonian by the solvent. Moreover, dynamical contributions to the properties generally will be different in the gas phase and in condensed phases. In other words, the difference between spectroscopic parameters computed on geometry minima, with respect to those averaged over the dynamics, will be dependent on the presence of the solvent.

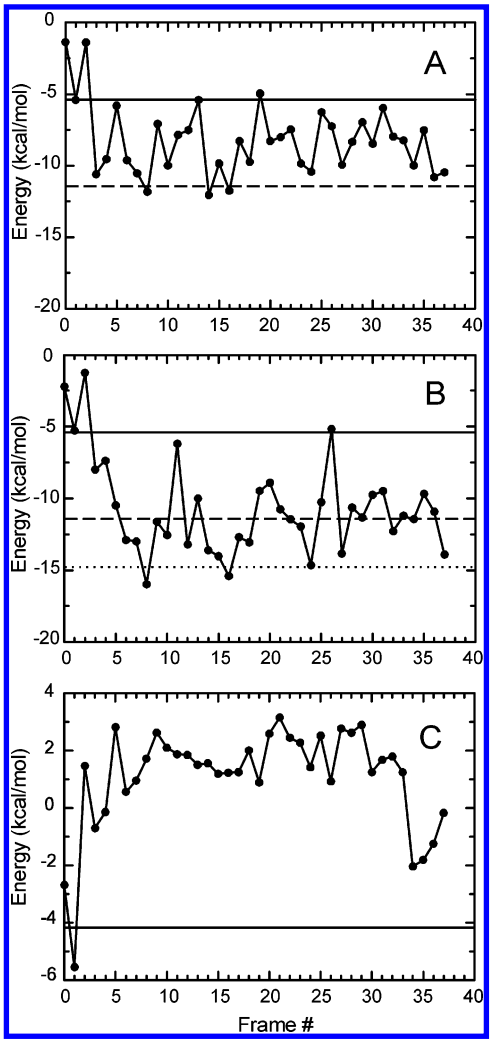

Figure 3. Energetic analysis of the carbonyl oxygen/water hydrogen bonds on 38 regularly spaced frames from the CPMD dynamics. The panels show the interaction energy of acetone with the two water molecules closest to the carbonyl oxygen (panel A) and the three water molecules (panel B) closest to carbonyl oxygen, as well as the interaction energy within the three-water cluster (panel C). In each panel, the horizontal lines indicate the energetic levels expected for a single hydrogen bond (solid line), two hydrogen bonds (dashed line), and three hydrogen bonds (dotted line), as determined from separate computations on optimized clusters.

To proceed in the analysis, we compared the average structure of acetone in aqueous solution, as obtained from the CPMD simulation, with optimized structures computed with alternative solvent models; of course, the Gaussian calculations used the same PBE functional that was used for CPMD. Not unexpectedly, the PCM alone proved unable to account for the entire geometrical effect of solvation; however, a satisfactory agreement was obtained by optimizing the acetone$-(H_2O)_2$ cluster, still in the presence of the PCM, with the same 6-31+G(d,p) basis set that has proven accurate in reproducing the gas-phase CPMD geometries (Table 4).

To date, we have focused on calculations, either at the CP/plane-wave level or with Gaussian basis sets, using the PBE functional: the main conclusion is that the cluster that is composed of acetone and two hydrogen-bonded water molecules, minimized in the presence of the PCM, can reproduce well the acetone geometrical changes that are observed between the gas-phase and the aqueous solution CPMD. To compute more-reliable structures, both in the gas phase and in solution, we can now shift to a hybrid functional such as PBE0, in

TABLE 4: Geometrical Parameters of Acetone from Different Solution Computations

	PBE/6-31+G(d,p)/PCM[a]		
	acetone	acetone−$(H_2O)_2$	CPMD[b]
	Bond Distance (Å)		
C═O	1.237 (+0.008)	1.247 (+0.018)	(+0.02)
C−C	1.511 (−0.009)	1.502 (−0.018)	(−0.02)
C−H	1.103 (+0.001)	1.103 (+0.001)	(0.00)
	Bond Angle (deg)		
C−C═O	121.6 (−0.6)	121.1 (−0.6)	(−0.5)
C−C−C	116.8 (+0.2)	117.8 (+1.2)	(+0.5)

[a] Values given in parentheses represent the difference, with respect to the gas-phase PBE/6-31+G(d,p) geometry of Table 2. [b] Values given in parentheses represent the difference, with respect to the CPMD gas-phase average geometry of Table 2.

TABLE 5: Geometrical Parameters for the Acetone Molecule, from PBE0/aug-cc-pVTZ Optimizations

	acetone PBE0/aug-cc-pVTZ	acetone−$(H_2O)_2$ PBE0/aug-cc-pVTZ/PCM[a]
	Bond Distance (Å)	
C═O	1.207	1.219 (+0.012)
C−C	1.506	1.498 (−0.008)
C−H	1.091	1.091 (0.00)
	Bond Angle (deg)	
C−C═O	121.8	121.3 (−0.5)
C−C−C	116.4	117.3 (+0.9)

[a] Values given in parentheses represent the difference, with respect to the gas-phase geometry.

combination with a large basis set. Table 5 shows the results of two such geometry optimizations: the first is that for an isolated acetone molecule, to simulate the gas-phase structure of acetone, and the second is that for the acetone−$(H_2O)_2$ cluster in the presence of PCM, to reproduce the structure of acetone in aqueous solution.

Apart from a difference in CH bond length, the parameters computed in vacuo match the experimental structure in the gas phase very well (see Table 1). Bond-length changes from the gas phase to the aqueous solution are slightly smaller than those extracted from the CPMD dynamics; however, this is consistent with the tendency of GGA functionals to overestimate bond lengths, which has been mentioned previously.

3.2. Spectroscopic Parameters. In the previously described analysis, we have not emphasized one of the main features of the water structure around the carbonyl, namely the strong asymmetry of the water distribution, with respect to the acetone molecular plane. Figure 4 depicts the heavy atoms of the clusters that are comprised of acetone and the two closest hydrogen-bonded waters, superimposed for a best fit of the acetone heavy atoms: there is a clear preference for the waters to lie close to the acetone molecular plane, as could be expected, based on chemical intuition.

Depending on the type of spectroscopic parameters one wishes to reproduce, the precise orientation of solvent molecules around the solute may turn out to be quite important. Thus, for example, Figure 5 shows the computed $n \rightarrow \pi^*$ transition energy, as well as ^{17}O magnetic shielding, for the cluster of acetone and two hydrogen-bonded waters, as a function of their angular displacement from the acetone molecular plane. The importance of an accurate weighting of the different hydrogen-bond orientations is apparent.

As we have shown recently, calculations where only a few water molecules closest to the carbonyl oxygen are treated explicitly at the DFT level, and the PCM cavity is built around

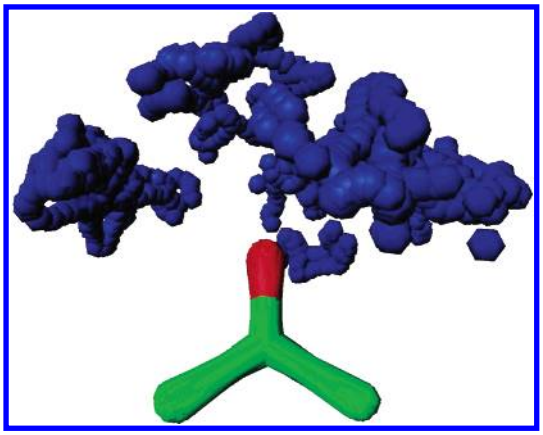

Figure 4. Overlap of acetone and hydrogen-bonded water clusters extracted from the CPMD. Water oxygens are shown in blue.

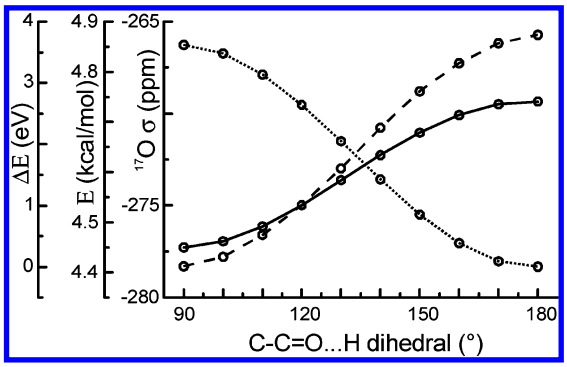

Figure 5. Computed $n \rightarrow \pi^*$ transition energy (solid line), ^{17}O NMR shielding (dashed line), and ground-state energy (dotted line) [PBE0/6-31+G(d,p)] for the cluster of acetone and two hydrogen-bonded water molecules, as a function of the angular displacement of the waters from the acetone molecular plane.

the resulting acetone/water clusters, provide essentially the same values for both the "blue shift" of the $n \rightarrow \pi^*$ UV transition[33a] and the ^{17}O nuclear magnetic shielding,[33b] as can be computed using much-larger clusters of explicit waters without recourse to the PCM.

However, these studies were focused more on the development of an accurate discrete/continuum approach than on the quality of the dynamics used to generate the acetone−water cluster configurations. As a matter of fact, cluster geometries were extracted from classical molecular dynamics (MD) simulations, using the AMBER force field.[34] Although the radial distribution of water around the carbonyl oxygen is reasonable, in the absence of appropriate force field modifications, any directionality of the hydrogen bonds is basically absent. This is contrary to the expected effect of the two sp^2 oxygen lone pairs in the molecular plane of acetone, as well as to the structural results from the much more accurate CP dynamics described previously.

Such structural features will definitely have an impact on the hydrogen-bond structure around the carbonyl: thus, it is quite conceivable that they may affect not only the value of the computed spectroscopic parameters, but also the level at which convergence, with respect to the number of explicit solvent molecules, is reached. Therefore, the entire issue of cluster size has been examined anew. Figure 6 plots the computed ^{17}O shielding, averaged on 38 evenly spaced frames from the CPMD trajectory, as a function of the number of water molecules included explicitly in the QM calculations: convergence is barely reached with 50 waters (at -260.4 ± 5.1 ppm). On the same plot, the dashed line corresponds to calculations using

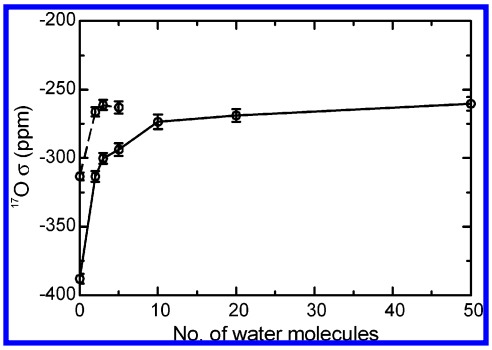

Figure 6. Average (38 frames from the solution CPMD simulation) acetone ^{17}O NMR shielding constants, computed at the PBE0/6-311+G(d,p) level, either in the absence (solid line) or in the presence (dashed line) of the PCM on acetone−water clusters of different size.

PCM, along with the reported number of explicit water molecules: with just two water molecules, the average shielding is already −266.3 ± 3.3 ppm, whereas, with three explicit waters, a value of −261.3 ± 3.7 ppm is reached, which is identical (within the uncertainty) to the QM reference.

The situation is quite similar in the case of the ^{13}C shielding, which is within 0.5 ppm of the QM reference with two explicit waters, and converges exactly at the level of three waters, and also for the $n \rightarrow \pi^*$ transition energy, where the PCM values with two and three waters differ by a mere 0.01 eV.

In conclusion, the choice of using three explicit waters (and possibly just two for the UV computations), in combination with the PCM model, is strongly supported. Thus, the three water molecules that, according to the structural analysis described previously, are needed to account for the direct hydrogen-bond network around the carbonyl oxygen in all CPMD frames, should also be included within the QM level of the NMR calculation, with the rest of the solvent being well-described by the PCM.

3.3. $n \rightarrow \pi^*$ Excitation Energy. The $n \rightarrow \pi^*$ electronic transition of acetone corresponds to the excitation of an electron from the nonbonding $2p_y$ orbital on the oxygen to the antibonding π^* molecular orbital on the carbonyl. For an acetone molecule in its C_2 or C_{2v} geometry, the transition is symmetry-forbidden; as a consequence of vibronic coupling, in the gas phase, a weak band at $\Delta E = 4.4-4.5$ eV is observed, with an oscillator strength of $f \approx 0.0004$.[35] In aqueous solution, the formation of acetone−water complexes breaks the C_{2v} symmetry, and the transition gains in strength by ∼50%; moreover, a shift toward higher excitation energies (a blue shift) is observed, which has been quantified to be in the range of 0.19−0.21 eV, and has been attributed to a ground-state stabilization by the solvent.[36]

In a recent paper,[33a] we have shown that a cluster/PCM approach can be used with success to rationalize the electronic structure of the acetone−water system; we found that, at least for the $^1A_2$ transition, the TD-DFT approach gives results that are consistent with other, more-expensive post-Hartree−Fock methods, and we decided to use PBE0 in combination with a locally dense basis set, namely, 6-311++G(2d,2p) on carbonyl and 6-31+G(d,p) on all other atoms; this basis set will be henceforth shortened as [6-311++G(2d,2p), 6-31+G(d,p)]. The consistency of this level of theory was tested on an acetone−$(H_2O)_2$ cluster extracted from a CPMD snapshot: the results are listed in Table 6.

In the present paper, we wish to extend a similar approach to take into account dynamical effects as well, using, as the starting point, the two CPMD simulations discussed in the preceding section. In the first stage, we examined the convergence of the average UV transition energies computed on an increasing number of frames (Figure 7).

TABLE 6: Basis Set Dependence of the ($n \rightarrow \pi^*$) Transition Energy Computed at the PBE0 Level for an Acetone−$(H_2O)_2$ Cluster

basis set	number of basis functions	$n \rightarrow \pi^*$ (eV)
6-31G	74	4.52
6-31G(d,p)	140	4.60
6-311G	108	4.54
6-311G(d,p)	168	4.61
6-311+G(2d)/6-31+G(d,p)	176	4.62
6-311+G(d,p)	192	4.62
6-311++G(2d,2p)	262	4.61
cc-pVTZ	320	4.60

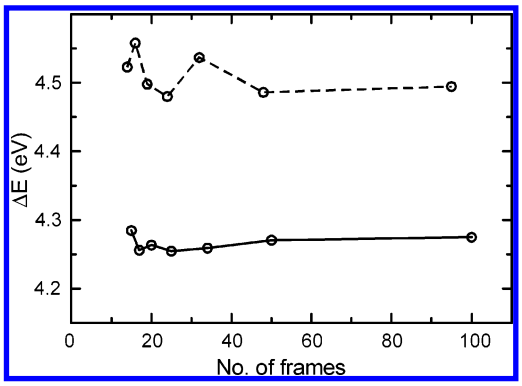

Figure 7. Average $\Delta E(n \rightarrow \pi^*)$ computed at the PBE0/[6-311++G(2d,2p), 6-31+G(d,p)] level on increasing numbers of evenly spaced CPMD frames. In vacuo calculations on the acetone molecule from the gas-phase CPMD (solid line) and PCM calculations on acetone + 3 H_2O clusters from the solution CPMD (dashed line) are shown.

A satisfactory convergence is reached at the level of ∼100 structures, which, in the case of our 40-ps CPMD runs, corresponds to a 40-fs time difference between individual frames. The other convergence issue that is encountered in the case of the aqueous solution computations—namely, the number water molecules that must be explicitly included in the cluster/PCM TD-DFT calculation—has been addressed in the preceding section, where we concluded that three water molecules represent a satisfactory choice for both UV and NMR computations. Table 7 lists the transition energies computed with this procedure and averaged over 100 frames of the solution CPMD, in comparison with the averages for the gas-phase CPMD and with the optimized geometries of Table 5.

As was the case for geometrical parameters, UV transition energies averaged over the CPMD trajectory agree well with the values computed on the PBE/6-31+G(d,p) minimum; the difference, with respect to the experimental transition energy, may be attributed to the uniform overestimation of bond distances that are associated with the use of a GGA functional. In support of this interpretation, the results obtained using the PBE0/aug-cc-pVTZ minimum energy structure instead are in good agreement with the experimental data. As far as the interpretation of solvation effects is concerned, Table 7 also reports a factorization into an indirect contribution, due to geometry relaxation, and a direct effect on the computed spectral property, which is associated with the actual presence of explicit water molecules and the PCM. The column labeled "acetone (in vacuo)" in Table 7 lists average transition energies computed in vacuo on the isolated acetone molecule at the geometries sampled during either the gas-phase or the aqueous-solution CPMD, as well as in some relevant minimum-energy structures;

TABLE 7: PBE0/[6-311++G(2d,2p), 6-31+G(d,p)] TD-DFT Calculation on Several Different Acetone and Acetone/Water Cluster Geometries

geometry	acetone (in vacuo)[a]	acetone/water clusters (PCM)[a]	transition energy (eV) $\Delta\Delta E_{ind}$	$\Delta\Delta E_{dir}$	$\Delta\Delta E_{tot}$
acetone PBE/6-31+G(d,p)	4.34				
acetone PBE0/aug-cc-pVTZ	4.48				
⟨acetone, gas-phase CPMD⟩	4.28 (0.02)				
acetone + 2 H_2O (acetone−$(H_2O)_2$) PBE/6-31+G(d,p) (PCM)	4.23	4.73	−0.11	0.50	0.39
acetone + 2 H_2O (acetone−$(H_2O)_2$) PBE0/aug-cc-pVTZ (PCM)	4.39	4.86	−0.09	0.47	0.38
⟨acetone + 3 H_2O (acetone−$(H_2O)_3$) clusters, aqueous solution CPMD⟩	4.15 (0.01)	4.49 (0.01)	−0.13	0.34	0.21
experimental[b]	∼4.5	∼4.7[c]			∼0.2

[a] Values given in parentheses represent the standard errors of the mean. [b] Data are taken from refs 35 and 36. [c] Aqueous solution.

the column labeled "acetone/water clusters (PCM)" in Table 7 contains values for the corresponding cluster/PCM calculations. Interestingly, note that the indirect shift measured on minimized clusters is comparable to that obtained from the CPMD: this strengthens the conclusion that cluster/PCM optimizations, at the theory level chosen, provide structures that are representative of aqueous solution geometries. However, it is also quite apparent that a single-point PCM calculation of the UV transition energy, that is performed on the acetone−$(H_2O)_2$ cluster at its PCM-optimized geometry, overestimates the solvation shift. This is not unexpected, from a physical viewpoint, because dynamical structural fluctuations will certainly cause the water molecules that are bound to the carbonyl to reach positions even rather far from the optimal geometry; as a matter of fact, only the values averaged over the CPMD account well for the experimental solvation blue shift. However, as far as absolute values for the transition energies are concerned, it should be stressed again that the CPMD averages are rather far from the values observed in experiment, and actually are worse than the absolute value computed on the PBE0/aug-cc-pVTZ/PCM optimized cluster.

To proceed further in the analysis, we will note, from Table 7, that the indirect solvation shift, $\Delta\Delta E_{ind}$ (i.e., the purely geometrical effect) is much the same in all three cases, with most of the change being related to the direct effect ($\Delta\Delta E_{dir}$). If we now subtract from the $\Delta\Delta E_{dir}$ computed on CPMD averages the corresponding figure for the PBE/6-31+G(d,p) minima, the result should essentially reflect a contribution from the dynamics of the two water molecules closest to the carbonyl oxygen. In other words, this is the difference in transition energy between a dynamical cluster and a static cluster with similar average geometrical properties; in the present case, $\Delta\Delta\Delta E_{dynamics}$ is approximately −0.2 eV. As the last step, we can now add this correction to the absolute transition energy computed on our best static acetone−$(H_2O)_2$ cluster, namely, that optimized at the PBE0/aug-cc-pVTZ/PCM level (4.86 eV), to get a final result (4.66 eV), which is in excellent agreement with the experiment (∼4.7 eV).

3.4. ^{17}O and ^{13}C Carbonyl Chemical Shifts. The ^{17}O magnetic shielding of the acetone oxygen changes by 75.5 ppm in going from the gas phase to aqueous solution,[33b] whereas the corresponding figure for the carbonyl carbon is −18.90 ppm.[37] The computation of such solvation shifts—and, in particular, the evaluation of the role of dynamical effects—has been addressed by an approach parallel to that described previously for the UV parameters. All of the DFT-GIAO calculations used the PBE0 functional, which has shown remarkable accuracy in many studies aimed at the calculation of NMR parameters, including carbon and oxygen shifts. A preliminary exploration of basis set convergence was performed on a specific acetone−$(H_2O)_2$ cluster extracted from the CPMD (Table 8); a satisfactory convergence requires a valence-triple-ζ basis set with diffuse and polarization functions. Similar to that in the case of the TD-DFT calculations, a locally dense basis set (6-311+G(d,p) on carbonyl and 6-31+G(d,p) on all other atoms) performs almost as well as the uniform 6-311+G(d,p); however, in view of the comparatively lower computational cost of NMR calculations, we decided to use the 6-311+G(d,p) basis set throughout the experiment. Again, convergence, with respect to the number of CPMD frames, is reached with ∼100 points (Figure 8).

TABLE 8: Basis-Set Dependence of the Absolute Magnetic Shieldings of the Carbonyl Atoms Computed at the PBE0 Level for an Acetone−$(H_2O)_2$ Cluster

basis set	number of basis functions	absolute magnetic shielding (ppm) ^{17}O	^{13}C
6-31G	74	−271.31	−22.54
6-31+G	98	−258.43	−23.80
6-31G(d,p)	140	−235.87	−20.36
6-311G	108	−312.07	−38.97
6-311G(d,p)	168	−279.52	−40.83
6-311+G(d,p)/6-31+G(d,p)	166	−273.87	−44.27
6-311+G(d,p)	192	−275.36	−43.90
6-311++G(2d,2p)	262	−274.92	−44.45
cc-pVTZ	320	−274.99	−43.32

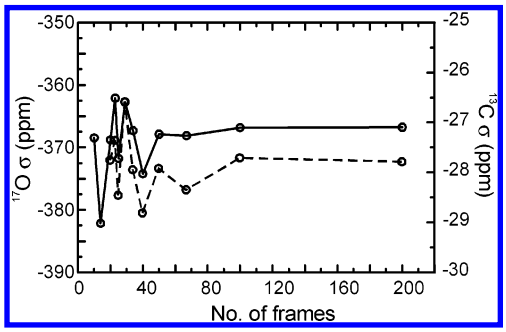

Figure 8. Average carbonyl ^{17}O (full line) and ^{13}C (dashed line) absolute magnetic shieldings (given in units of ppm) computed at the PBE0/6-311+G(d,p) level on increasing numbers of evenly spaced frames extracted from the gas-phase CPMD.

As was discussed in a previous section, two explicit water molecules in the PCM calculation provide rather satisfactory agreement with the reference full QM calculations, with the remaining difference being ∼8% of the total solvation shift, for both oxygen and carbon; however, a still better convergence is obtained with three explicit waters (to within 1% of the total solvation shift). The difference, with respect to the TD-DFT PCM computations, which were essentially converged with just two QM waters, should not come as a surprise, because some spectroscopic properties may well be more sensitive to the presence of explicit water molecules at specific positions. However, it is reassuring that the number of three water molecules, which, on the basis of structural and energetic

TABLE 9: PBE0/6-311+G(d,p) Gauge-Including Atomic Orbital (GIAO) Calculations on Several Different Acetone and Acetone + 3 H_2O Cluster Geometries

geometry	acetone (in vacuo)[a]	acetone/water clusters (PCM)[a]	GIAO shift (ppm) $\Delta\sigma_{ind}$	$\Delta\sigma_{dir}$	$\Delta\sigma_{tot}$
		^{17}O NMR Spectroscopy			
acetone PBE/6-31+G(d,p)	−366.7				
acetone PBE0/aug-cc-pVTZ	−339.0				
⟨acetone, gas-phase CPMD⟩	−367 (4)				
acetone + 2 H_2O (acetone−$(H_2O)_2$) PBE/6-31+G(d,p) (PCM)	−388.2	−243.9	−21.5	+144.3	+122.8
acetone + 2 H_2O (acetone−$(H_2O)_2$) PBE0/aug-cc-pVTZ (PCM)	−355.6	−238.2	−16.6	+117.4	+100.8
⟨acetone + 3 H_2O (acetone−$(H_2O)_3$), aqueous solution CPMD⟩	−390 (3)	−262 (3)	−23	+128	+105
experimental					+75.5
		^{13}C NMR Spectroscopy			
acetone PBE/6-31+G(d,p)	−26.6				
acetone PBE0/aug-cc-pVTZ	−19.2				
⟨acetone, gas-phase CPMD⟩	−27.9 (0.7)				
acetone + 2 H_2O (acetone−$(H_2O)_2$) PBE/6-31+G(d,p) (PCM)	−32.5	−48.0	−5.9	−15.5	−21.4
acetone + 2 H_2O (acetone−$(H_2O)_2$) PBE0/aug-cc-pVTZ (PCM)	−23.9	−42.0	−4.7	−18.1	−22.8
⟨acetone + 3 H_2O (acetone−$(H_2O)_3$), aqueous solution CPMD⟩	−34.7 (0.5)	−51.0 (0.6)	−6.8	−16.3	−23.1
experimental					−18.9

[a] Values given in parentheses represent the standard errors of the mean.

TABLE 10: Contributions to the Solvent Shifts of Carbonyl Atom Shielding Constants

	$\Delta\sigma_{ind} + \Delta\Delta\sigma_{geom}$[a]	$\Delta\sigma_{dir} + \Delta\Delta\sigma_{dynamics}$[b]	$\Delta\sigma_{tot}$
	^{17}O NMR Spectroscopy		
PBE0/aug-cc-pVTZ	−18	+101	+83
experimental			+75.5
	^{13}C NMR Spectroscopy		
PBE0/aug-cc-pVTZ	−5.6	−18.9	−24.5
experimental			−18.9

[a] $\Delta\Delta\sigma_{geom} = \Delta\sigma_{ind}$(CPMD) − $\Delta\sigma_{ind}$(PBE). [b] $\Delta\Delta\sigma_{dynamics} = \Delta\sigma_{dir}$(CPMD) − $\Delta\sigma_{dir}$(PBE).

consideration, was identified as necessary to describe the pattern of hydrogen bonds to carbonyl oxygen along the entire CPMD trajectory, is indeed a satisfactory choice for both NMR and UV.

Table 9 lists the absolute NMR shieldings averaged over the gas-phase and aqueous-solution CPMDs, in comparison with the values calculated on the reference minimum energy structures.

Magnetic shieldings computed on acetone at the PBE/6-31+G(d,p) minimum energy structure are in reasonable agreement with the corresponding gas-phase CPMD averages but are considerably different from the values obtained at the PBE0 geometry. As far as solvation effects are concerned, the PBE/6-31+G(d,p)/PCM optimized acetone−$(H_2O)_2$ cluster reproduces well the geometry-related indirect solvation effect ($\Delta\sigma_{ind}$), which is rather prominent in this case; however, the direct solvent effect on ^{17}O σ cannot be explained by a single acetone−water cluster. Instead, the total $\Delta\sigma$ value is best reproduced by the same procedure used for the $n \rightarrow \pi^*$ UV transition, i.e., by adding to the values computed on the most reliable minimum energy structure (PBE0/aug-cc-pVTZ) a correction that represents the difference between the CPMD average and the corresponding PBE/6-31+G(d,p) minima. The results of such a procedure are reported in Table 10.

4. Discussion and Conclusions

The present paper is devoted to an analysis of the different factors that have a role in the computation of reliable spectroscopic parameters for molecules in condensed phases. Taking acetone as an example, we have first shown that the PBE0 functional coupled to suitable basis sets provides accurate results for NMR and UV parameters in the gas phase: the favorable scaling properties of DFT will allow for the direct study of relatively large systems with a comparable accuracy. Next, we have shown that the PCM approach provides a means for the effective introduction of bulk solvent effects, which can be completed, for polar groups in hydrogen-bonding solvents, by explicit treatment of some first-shell solvent molecules. It is noteworthy in this connection that the replacement of these molecules by atomic charges (as is customary in QM/MM models) is dangerous: although, for some spectroscopic parameters, this procedure is sound and effective, it sometimes leads to disappointing results. Thus, for example, Table 11 compares the results obtained in the present case by a QM solute/MM solvent approach with those of the QM/PCM procedure presented previously.

TABLE 11: Average Computed Spectroscopic Parameters[a] from the Acetone−Water CPMD

number of waters	UV transition ($n \rightarrow \pi^*$) (eV)	σ (ppm) ^{17}O NMR	^{13}C NMR
60 MM	4.51	−270	−47.8
QM/PCM	4.49	−262	−51.0

[a] Average from 100 frames. The MM charges of water are those of the TIP3P model.[38] TD-DFT data were obtained at the PBE0/[6-311++G(2d,2p), 6-31+G(d,p)] level of theory, whereas NMR parameters were computed at the PBE0/6-311+G(d,p) level.

Although the UV transition energy is satisfactory at the QM/MM level, the magnetic shieldings are not fully explained by the purely electrostatic interaction. In view of the favorable scaling of DFT approaches mentioned previously, there is no compelling reason to avoid the treatment of this small number of water molecules at a QM level, possibly using locally dense basis sets. The resulting discrete/continuum model is very powerful and can be used also in a dynamic context, resorting to classical molecular dynamics or CPMD. Here again, some care must be exerted in regard to the choice of the approach, because different spectroscopic parameters can be sensitive to different details of dynamical fluctuations. For instance, rdfs are not always good indicators, because angular distribution around nonspherical groups can be equally important. Under such circumstances, direct use of ab initio dynamics or proper reparametrization of classical force fields can perform very good jobs. At the same time, even the computational level used in CP dynamics can be insufficient for the quantitative reproduction of spectroscopic parameters. Here again, the PCM comes into

play, because it allows us to replace "on the fly" computations on the entire solute/solvent system by more-refined computations on smaller cluster embedded in a polarizable continuum and averaged on a reduced number of frames. It is particularly gratifying in this connection that the number of explicit solvent molecules that must be included to obtain converged results is quite small and can be ascertained based on a combination of the usual geometrical analyses and of energetic criteria, e.g., by comparing the strength of solute−solvent interactions to the energy of the solvent dimer. Moreover, beyond this minimum, the choice of the actual number of explicit solvent molecules used is not very critical.

In summary, the integrated computational tool, consisting of the most recent hybrid density functionals, mixed discrete-continuum solvent models, hybrid QM/MM approaches, and averaging from molecular dynamics simulations, is becoming a valuable complement to experimental results. Furthermore, thanks to the implementation of all these items in user-friendly computer codes, this type of analysis also is or will shortly be feasible by nonspecialists and for much-larger molecules of biological and/or technological interest.

Acknowledgment. The authors thank the Italian Ministry for University and Research (MIUR) for financial support and the Sezione di Modelistica Computazionale of CIMCF at Naples for computer facilities.

References and Notes

(1) (a) Helgaker, T.; Jaszunski, M.; Ruud, K. *Chem. Rev.* **1999**, *99*, 293. (b) Merchan, M.; Serrano-Andres, L.; Fulscher, M. P.; Roos, B. O. *Recent Adv. Comput. Chem.* **1999**, *4*, 161. (c) Roos, B. O. *Acc. Chem. Res.* **1999**, *32*, 137. (d) Improta, R.; Barone, V. *Chem. Rev.* **2004**, *104*, 1231.

(2) (a) Goedecker, S.; Scuseria, G. E. *Comput. Sci. Eng.* **2003**, *5*, 14. (b) Scuseria, G. E. *J. Phys. Chem. A* **1999**, *103*, 4782.

(3) (a) P. Hohenberg, P.; Kohn, W. *Phys. Rev.* **1964**, *136*, B864. (b) Kohn, W.; Sham, L. J. *Phys. Rev.* **1965**, *140*, A1133.

(4) (a) Gross, E. K. U.; Kohn, W. *Phys. Rev. Lett.* **1985**, *55*, 2850. (b) Stratmann, R. E.; Scuseria, G. E.; Frish, M. J. *J. Chem. Phys.* **1998**, *109*, 8218. (c) Casida, M. E. In *Recent Advances In Density Functional Methods (Part I)*; Chong, D. P., Ed.; World Scientific: Singapore, 1994; pp 155−192.

(5) (a) Wolinski, K.; Hilton, J. F.; Pulay, P. *J. Am. Chem. Soc.* **1990**, *112*, 8251. (b) Helgaker, T.; Jaszunski, M.; Ruud, K. *Chem. Rev.* **1999**, *99*, 293. (c) Cheeseman, J. R.; Trucks, G. W.; Keith, T. A.; Frisch, M. J. *J. Chem. Phys.* **1998**, *104*, 5497.

(6) (a) Crescenzi, O.; Correale, G.; Bolognese, A.; Piscopo, V.; Parrilli, M.; Barone, V. *Org. Biomol. Chem.* **2004**, *1*, 1577.

(7) (a) Bagno, A.; Rastrelli, F.; Sacelli, G. *J. Phys. Chem. A* **2003**, *107*, 9964. (b) Giesen, D. J.; Zumbulyadis, N. *Phys. Chem. Chem. Phys.* **2002**, *4*, 5498. (c) Benzi, C.; Cossi, M.; Barone, V. *Phys. Chem. Chem. Phys.* **2004**, *6*, 2557. (d) Benzi, C.; Crescenzi, O.; Pavone, M.; Barone, V. *Magn. Res. Chem.* **2004**, *42*, S57−S67.

(8) (a) Persico, M.; Tomasi, J. *Chem. Rev.* **1994**, *94*, 2027. (b) Cramer, C. J.; Truhlar, D. G. *Chem. Rev.* **1999**, *99*, 2161.

(9) (a) Iwata, S.; Morokuma, K. *J. Am. Chem. Soc.* **1975**, *97*, 966. (b) Kraus, M.; Webb, S. P. *J. Chem. Phys.* **1997**, *107*, 5771.

(10) Gauss, J. *J. Chem. Phys.* **1993**, *99*, 3629. (b) Gauss, *J. Phys. Chem. Chem. Phys.* **1995**, *99*, 1001. (c) Stratmann, R. E.; Scuseria, G. E.; Frisch, M. J. *J. Chem. Phys.* **1998**, *109*, 8218.

(11) Miertus, S.; Scrocco, E.; Tomasi, J. *Chem. Phys.* **1981**, *55*, 117.

(12) (a) Cossi, M.; Scalmani, G.; Rega, N.; Barone, V. *J. Chem. Phys.* **2002**, *117*, 43. (b) Scalmani, G.; Barone, V.; Kudin, K. N.; Pomelli, C. S.; Scuseria, G. E.; Frisch, M. J. *Theor. Chem. Acc.* **2004**, *111*, 90. (c) Barone, V.; Cossi, M.; Tomasi, J. *J. Chem. Phys.* **1997**, *107*, 3210. (d) Cossi, M.; Barone, V. *J. Phys. Chem. A* **2000**, *104*, 10614.

(13) (a) Adamo, C.; Cossi, M.; Rega, N.; Barone, V. In *Theoretical Biochemistry: Processes and Properties of Biological Systems*; Theoretical and Computational Chemistry, Vol. 9; Elsevier: New York, 1999. (b) Cossi, M.; Barone, V. *J. Chem. Phys.* **2000**, *112*, 2427. (c) Cossi, M.; Barone, V. *J. Chem. Phys.* **2001**, *115*, 4708.

(14) (a) Adamo, C.; Barone, V. *Chem. Phys. Lett.* **2000**, *320*, 152. (b) Aquilante, F.; Roos, B.; Barone, V. *J. Chem. Phys.* **2003**, *119*, 12323.

(15) (a) Canuto, S.; Coutinho, K.; Zerner, M. *J. Chem. Phys.* **2000**, *112*, 7293. (b) Coutinho, K.; Canuto, S. *J. Chem. Phys.* **2000**, *113*, 9132. (c) Coutinho, K.; Canuto, S. *J. Mol. Struct. (THEOCHEM)* **2003**, *632*, 235.

(16) Car, R.; Parrinello, M. *Phys. Rev. Lett.* **1985**, *55*, 2471.

(17) Bernasconi, L.; Sprik, M.; Hutter, J. *J. Chem. Phys.* **2003**, *119*, 12417.

(18) Rohrig, U. F.; Frank, I.; Hutter, J.; Laio, A.; VandeVondele, J.; Rothlisberger, U. *Chem. Phys. Chem.* **2003**, *4*, 1177.

(19) (a) Adamo, C.; di Matteo, A.; Barone, V. *Adv. Quantum Chem.* **1999**, *36*, 45. (b) Pavone, M.; Barone, V.; Ciofini, I.; Adamo, C. *J. Chem. Phys.* **2004**, *120*, 9167.

(20) (a) Sebastiani, D.; Parrinello, M. *J. Phys. Chem. A* **2001**, *105*, 1951. (b) Bühl, M. *J. Chem. Phys. A* **2002**, *106*, 10505.

(21) (a) Giannozzi, P.; De Angelis, F.; Car, R. *J. Chem. Phys.* **2004**, *120*, 5903. (b) Pasquarello, A.; Laasonen, K.; Car, R.; Lee, C.; Vanderbilt, D. *Phys. Rev. Lett.* **1992**, *69*, 1982.

(22) Perdew, J. P.; Burke, K.; Ernzerhof, M. *Phys. Rev. Lett.* **1996**, *77*, 3865.

(23) Vanderbilt, D. *Phys. Rev. B* **1990**, *41*, 7892.

(24) (a) Hetenyi, B.; De Angelis, F.; Giannozzi, P.; Car, R. *J. Chem. Phys.* **2004**, *120*, 8632. (b) Silvestrelli, P. L.; Parrinello, M. *J. Chem. Phys.* **1999**, *111*, 3572. (c) Silvestrelli, P. L.; Parrinello, M. *Phys. Rev. Lett.* **1999**, *82*, 3308.

(25) Nosé, S. *J. Chem. Phys.* **1984**, *81*, 511.

(26) Frisch, M. J.; Trucks, G. W.; Schlegel, H. B.; Scuseria, G. E.; Robb, M. A.; Cheeseman, J. R.; Montgomery, J. A., Jr.; Vreven, T.; Kudin, K. N.; Burant, J. C.; Millam, J. M.; Iyengar, S. S.; Tomasi, J.; Barone, V.; Mennucci, B.; Cossi, M.; Scalmani, G.; Rega, N.; Petersson, G. A.; Nakatsuji, H.; Hada, M.; Ehara, M.; Toyota, K.; Fukuda, R.; Hasegawa, J.; Ishida, M.; Nakajima, T.; Honda, Y.; Kitao, O.; Nakai, H.; Klene, M.; Li, X.; Knox, J. E.; Hratchian, H. P.; Cross, J. B.; Adamo, C.; Jaramillo, J.; Gomperts, R.; Stratmann, R. E.; Yazyev, O.; Austin, A. J.; Cammi, R.; Pomelli, C.; Ochterski, J. W.; Ayala, P. Y.; Morokuma, K.; Voth, G. A.; Salvador, P.; Dannenberg, J. J.; Zakrzewski, V. G.; Dapprich, S.; Daniels, A. D.; Strain, M. C.; Farkas, O.; Malick, D. K.; Rabuck, A. D.; Raghavachari, K.; Foresman, J. B.; Ortiz, J. V.; Cui, Q.; Baboul, A. G.; Clifford, S.; Cioslowski, J.; Stefanov, B. B.; Liu, G.; Liashenko, A.; Piskorz, P.; Komaromi, I.; Martin, R. L.; Fox, D. J.; Keith, T.; Al-Laham, M. A.; Peng, C. Y.; Nanayakkara, A.; Challacombe, M.; Gill, P. M. W.; Johnson, B.; Chen, W.; Wong, M. W.; Gonzalez, C.; Pople, J. A. *Gaussian 03*, revision C.02; Gaussian, Inc.: Pittsburgh, PA, 2004.

(27) Adamo; C., Barone, V. *J. Chem. Phys.* **1999**, *110*, 6158.

(28) Francl, M. M.; Petro, W. J.; Hehre, W. J. S.; Binkley, J.; Gordon, M. S.; DeFrees, D. J.; Pople, J. A. *J. Chem. Phys.* **1982**, *77*, 3654.

(29) Dunning, T. H., Jr. *J. Chem. Phys.* **1989**, *90*, 1007.

(30) Hilderbrandt, R. L.; Andreassen, A. L.; Bauer, S. H. *J. Phys. Chem.* **1970**, *74*, 1586.

(31) Gibson, D. A.; Ionova, I. V.; Carter, E. A. *Chem. Phys. Lett.* **1995**, *240*, 261.

(32) Ferrario, M.; Haughney, M.; McDonald, I. R.; Klein, M. L. *J. Chem. Phys.* **1990**, *93*, 5156.

(33) (a) Aquilante, F.; Cossi, M.; Crescenzi, O.; Scalmani, G.; Barone, V. *Mol. Phys.* **2003**, *101*, 1945. (b) Cossi, M.; Crescenzi, O. *J. Chem. Phys.* **2003**, *118*, 8863.

(34) Cornell, W. D.; Cieplak, P.; Bayly, C. I.; Gould, I. R.; Merz, K. M., Jr.; Ferguson, D. M.; Spellmeyer, D. C.; Fox, T.; Caldwell, J. W.; Kollman, P. A. *J. Am. Chem. Soc.* **1995**, *117*, 5179.

(35) (a) Merchan, M.; Roos, B. O.; McDiarmid, R.; Xing, X. J. *J. Chem. Phys.* **1996**, *104*, 1791. (b) Hess, B.; Bruna, P. J.; Buenker, R. J.; Peyerimhoff, S. D. *Chem. Phys.* **1976**, *18*, 267. (c) McMurry, H. L. *J. Chem. Phys.* **1941**, *9*, 231.

(36) (a) Bayliss, N. S.; McRae, E. G. *J. Phys. Chem.* **1954**, *58*, 1006. (b) Balasubramanian, A.; Rao, C. N. R. *Spectrochim. Acta* **1962**, *18*, 1337. (c) Bayliss, N. S.; Wills-Johnson, G. *Spectrochim. Acta A* **1968**, *24*, 551.

(37) Tiffon, B.; Dubois, J. E. *Org. Magn. Res.* **1978**, *11*, 295.

(38) Jorgensen, W. L.; Chandrasekhar, J.; Madura, J. D.; Impey, R. W.; Klein, M. L. *J. Chem. Phys.* **1983**, *79*, 926.